Journal of Power Sources 185 (2008) 649–655

Contents lists available at ScienceDirect

Journal of Power Sources

journal homepage: www.elsevier.com/locate/jpowsour

Improvement of $(La_{0.74}Bi_{0.10}Sr_{0.16})MnO_3$–$Bi_{1.4}Er_{0.6}O_3$ composite cathodes for intermediate-temperature solid oxide fuel cells

Junliang Li, Shaorong Wang*, Xiufu Sun, Renzhu Liu, Xiaofeng Ye, Zhaoyin Wen

Shanghai Institute of Ceramics, Chinese Academy of Sciences, 1295 Dingxi Road, Shanghai 200050, PR China

ARTICLE INFO

Article history:
Received 3 July 2008
Received in revised form 1 September 2008
Accepted 1 September 2008
Available online 16 September 2008

Keywords:
Intermediate-temperature solid oxide fuel cells
Cathode stability
Impedance spectroscopy
Composite cathode

ABSTRACT

Porous composite cathodes including $(La_{0.74}Bi_{0.10}Sr_{0.16})MnO_{3-\delta}$ (LBSM) and $Bi_{1.4}Er_{0.6}O_3$ (ESB) were fabricated and characterized using AC impedance spectroscopy. In our earlier work, the growth and aggregation of ESB particles were found in LBSM–ESB composite cathodes. In this study, therefore, two approaches were used to restrain the growth and aggregation of ESB particles. First, the sintering temperature of the composite cathode was reduced by introducing a sintering function layer, which caused a 22% reduction in the initial polarization resistance (R), but the cathode polarization resistance decreased at a rate of $2.15 \times 10^{-4}\ \Omega\,cm^2\,h^{-1}$ at 700 °C during a period of 100 h. Second, nano-sized Gd-doped ceria powder (CGO) was added to the composite cathode system. Stability improvement was achieved at 10 vol% CGO, and the degradation rate at 700 °C was $4.01 \times 10^{-5}\ \Omega\,cm^2\,h^{-1}$ during a period of 100 h.

1. Introduction

The solid oxide fuel cell (SOFC) is the most efficient device invented to date for the conversion of chemical fuels directly into electrical power [1,2]. A significant improvement in the recent development of the SOFC is the reduction of its operating temperature from above 800 °C to a range of 650–800 °C [3]. Unfortunately, the cathode polarization resistance increases rapidly when the operating temperature is reduced [4,5]. Activation polarization is typically more of an issue in cathodes than in anodes, due primarily to the kinetics of the oxygen reduction reaction (attributable to the high bond strength present in oxygen molecules), which is several orders of magnitude slower than the reactions involving fuel oxidation [6–12]. In cathodes, the dissociative adsorption of oxygen is a thermally activated process [13]—as the operating temperature is decreased, the rates of chemical reactions are decreased dramatically, and activation polarization at the cathode becomes an even larger issue. Therefore, the composition of the cathode has a critical role in establishing cell operating temperatures.

Bismuth-based composite cathodes, such as Ag-ESB ($Bi_{0.8}Er_{0.2}O_{1.5}$) [14,15], Ag-YSB ($Bi_{0.75}Y_{0.25}O_{1.5}$) [16,17], and $Bi_2Ru_2O_7$ (-ESB), exhibit good performance at intermediate temperatures [18,19]. Conductors based on bismuth oxide have a much greater conductivity of oxygen ions, and the conductivity of bismuth oxide is approximately two orders of magnitude greater than that of stabilized zirconia. A further advantage of Bi_2O_3 is its favorable catalytic effect on oxygen dissociation, which is always the first, and often limiting, step in every electrochemical process involving oxygen transfer. For example, the area-specific resistance of $Bi_2Ru_2O_7$ and $Bi_2Ru_2O_7$-ESB cathodes at 700 °C was as low as $0.4\ \Omega\,cm^2$ and $0.03\ \Omega\,cm^2$, respectively [18,19]. Cathodes composed of $(La_{0.74}Bi_{0.10}Sr_{0.16})MnO_{3-\delta}$ (LBSM) and $Bi_{1.4}Er_{0.6}O_3$ (ESB) were studied in our earlier work, and the lowest area-specific resistance at 700 °C was only $0.21\ \Omega\,cm^2$ [20]. However, long-term tests of LBSM–ESB cathodes are needed because of the potential growth and aggregation of the ESB particles at operating temperatures, and the goal of this study was to improve the stability of this cathode system.

2. Experimental

LBSM powder was synthesized by autoignition of citrate–nitrate gel, and ESB powder was synthesized by the conventional solid state reaction, as described [20].

Firstly, the sintering function layers were prepared by screen printing slurries of ESB onto both sides of Sc-stabilized zirconia (ScSZ) electrolyte slices and sintering at 850 °C for 6 h in air to give the structure ESB/ScSZ/ESB. Next, slurries of LBSM–ESB (50 vol% ESB) were screen printed onto each side of the ESB/ScSZ/ESB slices, and sintered at various temperatures (750 °C, 800 °C, and 850 °C) for 2 h in air to fabricate the symmetric cells for the impedance study. Secondly, the LBSM–ESB–CGO (the nano-sized

* Corresponding author. Tel.: +86 21 52411520; fax: +86 21 52413903.
E-mail address: srwang@mail.sic.ac.cn (S. Wang).

0378-7753/$ – see front matter © 2008 Elsevier B.V. All rights reserved.
doi:10.1016/j.jpowsour.2008.09.012

Table 1
Polarization resistance of LBSM–ESB at various temperatures.

Cathode sintering temperature	R (Ω cm^2) at different temperatures				
	750 °C	700 °C	650 °C	600 °C	550 °C
750 °C	0.100	0.175	0.380	0.969	2.658
800 °C	0.086	0.165	0.368	0.942	2.620
850 °C	0.126	0.218	0.463	1.148	3.147

CGO powder was provided by Rare-Chem Hi-Tech Co., Ltd.) mixtures were prepared by mixing LBSM powder (50 vol%) with ESB and CGO: 45 vol%, 40 vol%, 35 vol%, 30 vol% for ESB corresponds to 5 vol%, 10 vol%, 15 vol%, 20 vol% for CGO, and the mixtures are named LBSM–ESB–CGO5, LBSM–ESB–CGO10, LBSM–ESB–CGO15, and LBSM–ESB–CGO20, respectively. The symmetric cells were fabricated by screen printing using LBSM–ESB–CGO and ScSZ as cathodes and electrolytes, respectively, and sintered at 900 °C for 2 h in air. The area of each electrode was 1 cm^2. Silver mesh, attached to the cathode surface with silver paste, was used as the current collector. A four-probe configuration was used for electrochemical impedance spectroscopy (EIS) measurements.

The electrochemical performance of the cathodes was characterized at various temperatures in air by EIS at open circuit, using AC impedance spectroscopy (ZAHNER IM6e) with a 20 mV AC signal, over a frequency range of 0.05 Hz to 1 MHz. The microstructure of the cathode/electrolyte section was studied by scanning electron microscopy (SEM). Various phases of the powder were identified with a Rigaku X-ray diffraction (XRD) diffractometer at room temperature, using monochromatic Cu Kα radiation.

3. Results and discussion

3.1. Effect of the sintering function layer

As each reaction is affected by the microstructure of the electrode, the sintering temperature has a significant influence on the electrode polarization resistance. In our earlier work, we observed that sintering at 900 °C resulted in the minimum polarization resistance for the LBSM–ESB composite cathode on the ScSZ electrolyte, but there was excessive growth of ESB particles [20]. The performance of an LBSM–ESB cathode can be improved by limiting the growth and aggregation of ESB particles; so, the ESB sintering function layer was introduced between the composite cathode and the ScSZ electrolyte (ScSZ/ESB/LBSM–ESB) in order to reduce the cathode sintering temperatures. Table 1 gives the total polarization resistance of the LBSM–ESB cathode on the ESB sintering function layer. It was noted that sintering at 800 °C resulted in the minimum polarization resistance (R). Fig. 1 shows the impedance spectra of the LBSM–ESB cathode sintered at 800 °C for 2 h on the ESB sintering function layer and then measured in air at various temperatures. The character of the impedance spectra was similar to that of the LBSM–ESB cathode on the ScSZ electrolyte, where the polarization resistance was attributed to oxygen adsorption and desorption on the electrode surface and the diffusion of oxygen ions [20].

Fig. 2 shows the typical microstucture of the ScSZ/ESB/LBSM–ESB half cell. Fig. 3a–f shows the cross-section SEM images of cathodes sintered at various temperatures on the ESB sintering function layers. As shown in Fig. 2, the ESB sintering function layer is dense and integrates with the ScSZ electrolyte. At 750 °C (the cathode sintering temperature), the contact between the LBSM–ESB cathode and the ESB layer is poor, as shown in Fig. 3a. Its high level of polarization resistance may be attributed tentatively to the poor contact due to the low sintering temperature. Similar phenomena have been observed for the LSM–YSZ composite cathode [21]. When the cathode sintering temperature was increased to 800 °C or 850 °C, contact between the LBSM–ESB cathode and the ESB layer became strong, as shown in Figs. 3c and e. It can be seen in Figs. 3b and d that the size of the ESB particles in the composite cathodes sintered at 750 °C and at 800 °C is about 1 μm in diameter, although there is some growth of ESB particles when the sintering temperature is 800 °C. The porosity of the composite cathode was acceptable, and LBSM–ESB sintered at 800 °C yielded a relatively low polarization resistance. But at sintering temperatures up to 850 °C, as shown in Fig. 3f, the ESB particle size increased to about 2 μm and the ESB particles were partially aggregated with increased sintering temperature. In this case, the increase of polarization resistance might

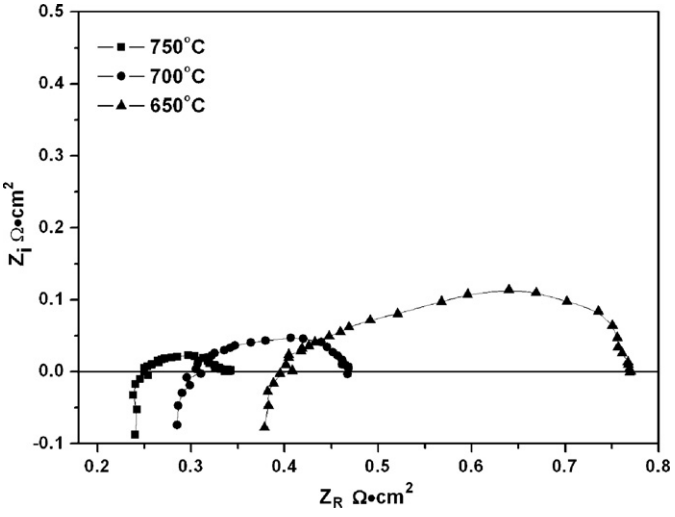

Fig. 1. AC impedance spectra measured at 650 °C, 700 °C, and 750 °C for LBSM–ESB sintered at 800 °C for 2 h on the ESB sintering function layer.

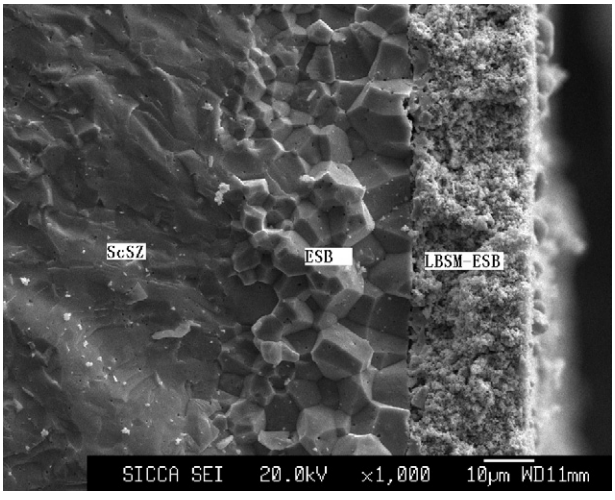

Fig. 2. Typical microstructure of the ScSZ/ESB/LBSM–ESB half cell.

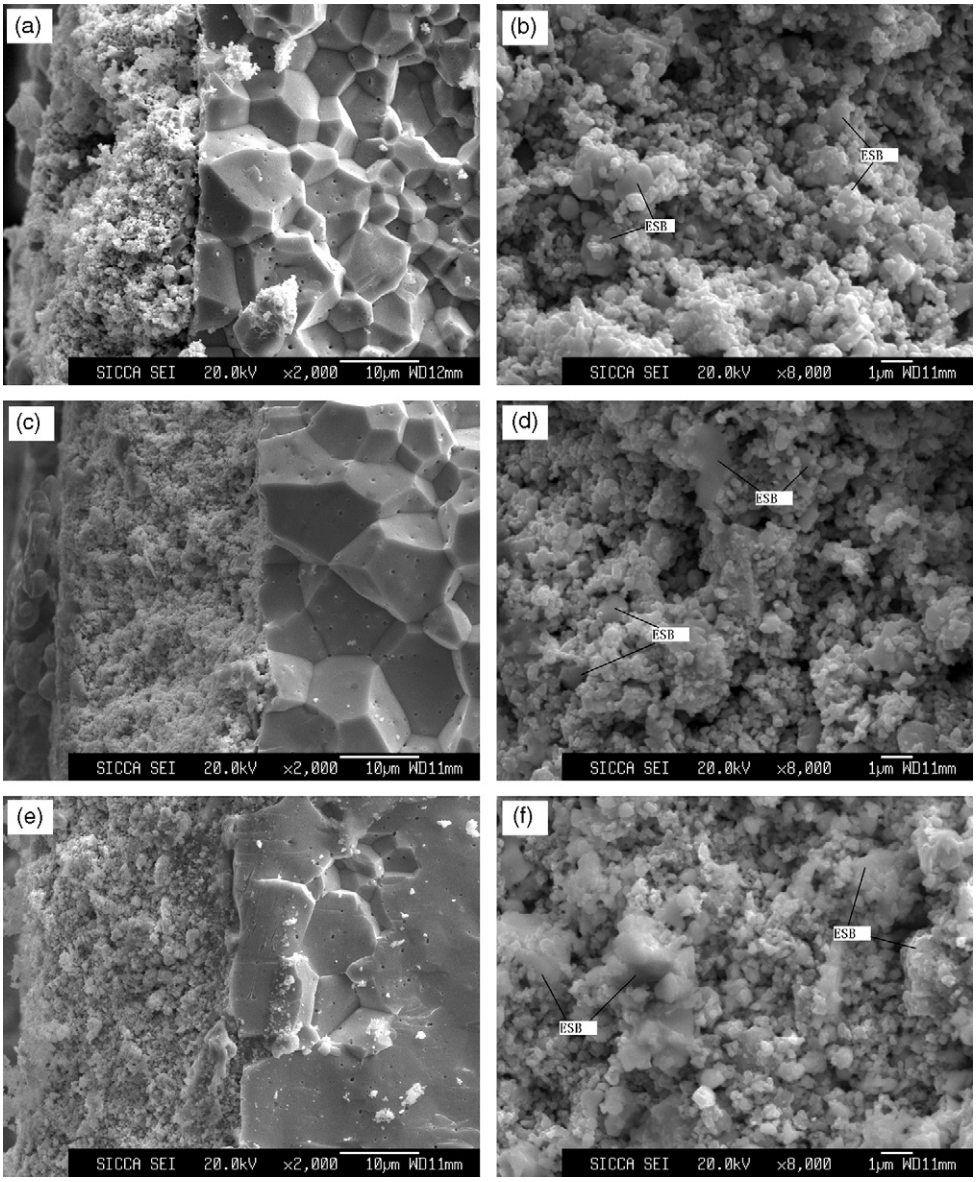

Fig. 3. Typical SEM fracture cross-section images of LBSM–ESB cathodes sintered at 750 °C (a and b), 800 °C (c and d), and 850 °C (e and f) for 2 h on the ESB sintering function layer.

be due to further growth and agglomeration of the ESB particles, which decreased the cathode porosity and reduced the gas diffusion rate. The triple phase boundaries (TPBs) in the LBSM–ESB cathode and on the cathode–electrolyte interface were also decreased. Consequently, the performance was weakened and the cathode had a higher polarization resistance.

3.2. Effect of the GDC particles

The second attempt to improve the performance of this composite cathode system involved the use of nano-sized CGO particles. Nano-sized CGO powder was used in this study as it is readily available, has relatively high ionic conductivity and sintering temperature, and is non-reactive toward LBSM or ESB at the temperature range of interest. Fig. 4 summarizes the total polarization resistances (R) for each of the LBSM–ESB–CGO cathodes measured in air. In general, the total polarization resistance (R) decreased as the CGO content increased to 10 vol%; however, values of R increased for a further addition of CGO up to 15 vol% or 20 vol%. This may be because the oxygen ionic conductivity of the CGO substitute is lower than that of ESB, and hence there is a decrease in ionic transfer rate in the composite cathodes. For instance, the LBSM–ESB–CGO5 cathode yielded $R = 0.295\ \Omega\,cm^2$ at 700 °C. The optimal composition, LBSM–ESB–CGO10, yielded $R = 0.177\ \Omega\,cm^2$ at 700 °C, and the LBSM–ESB–CGO15 cathode yielded $R = 0.208\ \Omega\,cm^2$ at 700 °C, whereas LBSM–ESB prepared on the ScSZ electrolyte yielded $R = 0.21\ \Omega\,cm^2$ at 700 °C [20]. The polarization resistance of LBSM–ESB–CGO10 was a littler lower than that of the LBSM–ESB cathode on the ScSZ electrolyte.

Fig. 5a–d shows typical SEM cross-section images of cathodes sintered on the ScSZ electrolyte at 900 °C for 2 h. As shown in Fig. 5a, some ESB particles grew and were partially aggregated in the LBSM–ESB–CGO5 cathode. The particles in the LBSM–ESB–CGO10 cathode are relatively homogeneous, as shown in Fig. 5b, and there is no obvious aggregation phenomenon. The polarization resistance of this cathode system is lower than that of LBSM–ESB prepared on the ScSZ electrolyte, which can be explained, at least in part, by the homogeneous distribution of the particles in this cathode. In this

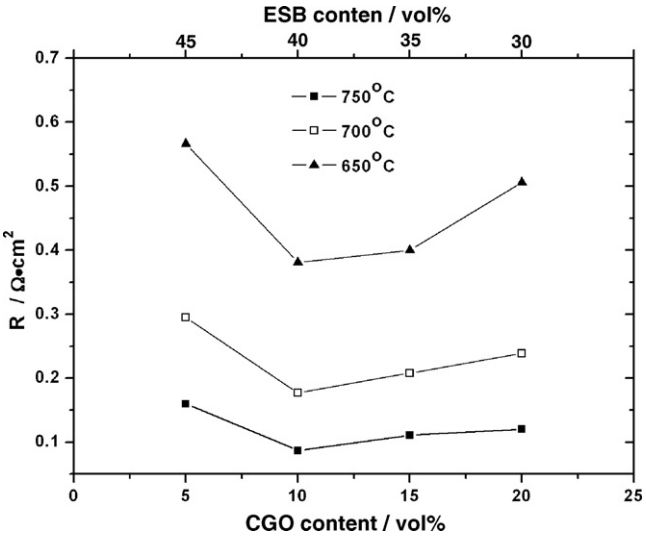

Fig. 4. Polarization resistance of LBSM–ESB–CGO cathodes with various contents of ESB and CGO.

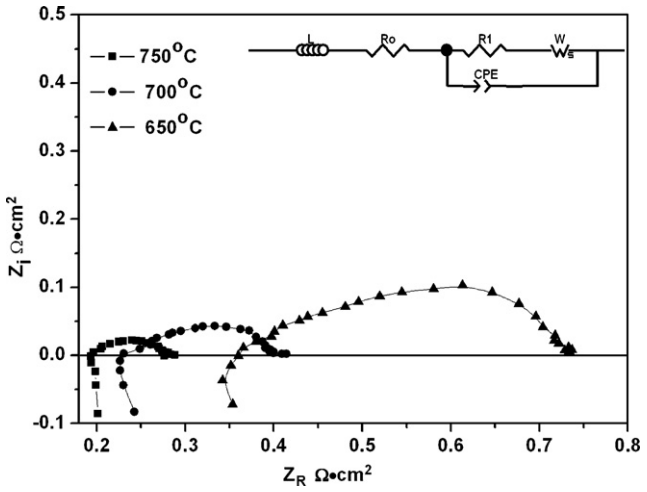

Fig. 6. AC impedance spectra measured at 650 °C, 700 °C, and 750 °C for LBSM–ESB–CGO10 sintered at 900 °C for 2 h. The corresponding equivalent circuit is shown.

case, the uniform distribution of the electronic conducting particles and the ionic conducting particles in the composite cathode provided the effective ionic and electronic conducting pathways, which effectively extended the TPB and, at the same time, promoted the synergistic process involving the injection of the mobile charged oxygen species into the ionic carriers. When the CGO content was 20 vol%, the particles in the LBSM–ESB–CGO20 cathode became more homogeneous, as shown in Fig. 5c, which was of great benefit for higher levels of cathode stability. However, as shown in Fig. 5d, the combination of the composite cathode and the electrolyte is relatively weak, which increased the interface polarization resistance and decreased the cathode stability.

Fig. 6 shows the impedance spectra of the LBSM–ESB–CGO10 cathode that was sintered at 900 °C for 2 h on the ScSZ electrolyte and then measured in air at various temperatures. It is noteworthy that the impedance spectra include a depressed semicircle in the low-frequency section and a minor high-frequency arc, similar to the LBSM–ESB cathode on the ScSZ electrolyte [20]. The low-frequency semicircle comprises the chief contributing element in Fig. 6. It has been suggested that the low-frequency semicircle can be attributed to oxygen adsorption and desorption

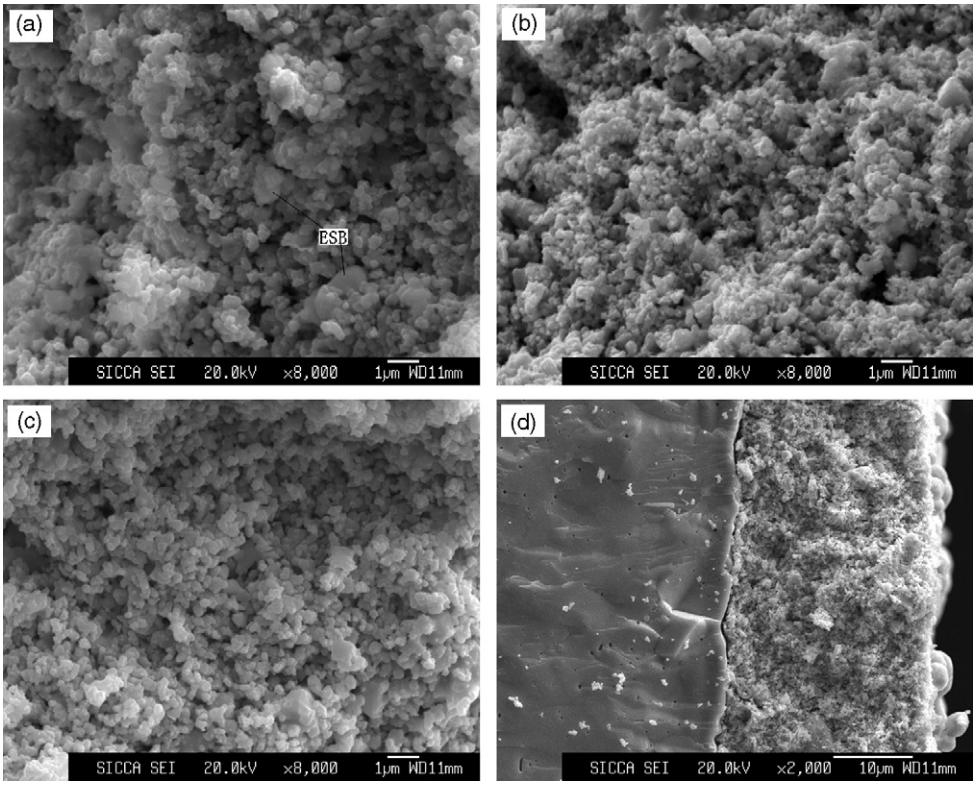

Fig. 5. Typical SEM fracture cross-section images of LBSM–ESB–CGO5 (a), LBSM–ESB–CGO10 (b), LBSM–ESB–CGO20 (c) and (d) cathodes sintered at 900 °C for 2 h on the ScSZ electrolyte.

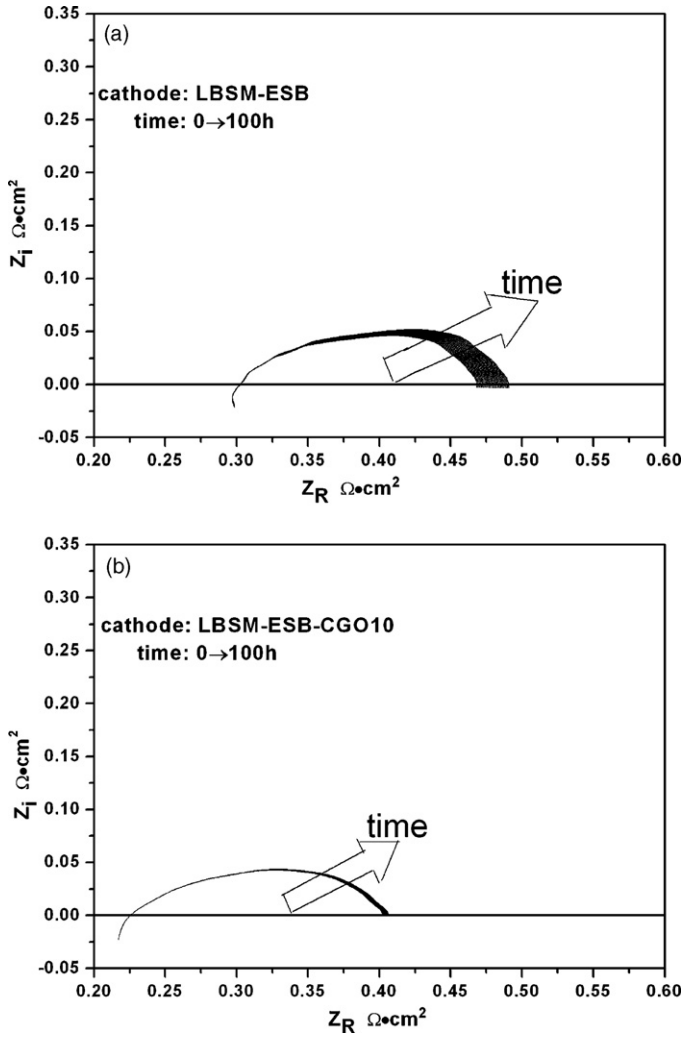

Fig. 7. AC impedance spectra obtained from symmetrical LBSM–ESB/ESB/ScSZ/ESB/LBSM–ESB (a) and LBSM–ESB–CGO10/ScSZ/LBSM–ESB–CGO10 (b) at 700 °C over a period of 100 h.

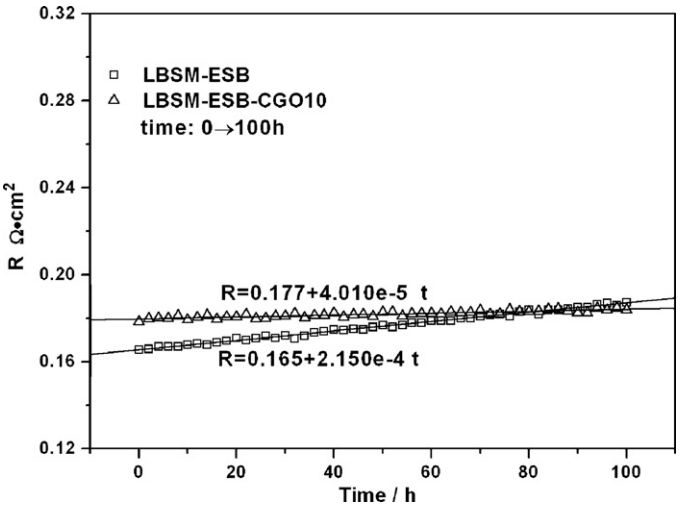

Fig. 8. Cathode polarization resistances (R) vs. time for LBSM–ESB and LBSM–ESB–CGO10 at 700 °C.

on the electrode surface, and the diffusion of oxygen ions [22–24]. On the other hand, the high-frequency arc can be attributed to polarization during charge transfer. In the equivalent circuit, the inductance L is attributed to high-frequency artifacts arising from the measurement apparatus. The first resistance (R_0) corresponds to the resistance of the electrolyte and the lead wires. The second resistance (R_1) is interpreted as the charge transfer resistance, which is contributed by electrochemical reaction at the cathode–electrolyte interface. Values of R_1 at 650 °C, 700 °C, and 750 °C for this cathode were 0.086 Ω cm², 0.031 Ω cm², and 0.013 Ω cm², respectively. The Warburg impedance (W) is related to the resistance of oxygen adsorption/decomposition and the diffusion of oxygen ions in the cathode. Values of W at 650 °C, 700 °C and 750 °C for this cathode were 0.295 Ω cm², 0.146 Ω cm² and 0.074 Ω cm², respectively. The percentage for W in the total polarization resistance of the composite cathode decreased with increased measurement temperature. The value for capacitance of the constant phase element (CPE) was about 10^{-3} F, and varied weakly with temperature in this composite cathode.

3.3. Long-term performance of the composite cathodes

The impedance spectra for the long-term tests of the LBSM–ESB (sintered at 800 °C on the ESB sintering function layer) and the LBSM–ESB–CGO10 (sintered at 900 °C on the ScSZ electrolyte) systems at 700 °C are shown in Fig. 7. It is clear from this figure that the electrode polarization for each system increased with time. Electrode polarization resistance (R) is plotted against time for the two systems at 700 °C in Fig. 8. The LBSM–ESB electrode on the ESB sintering function layer exhibited lower resistance than the LBSM–ESB–CGO10 cathode at the initial time, which could be due to the higher ionic conductivity of the ESB phase than CGO. In addition, since the LBSM–ESB electrode study was performed on the ESB sintering function layer, which had the same composition as the ionic conducting phase in the electrode, the polarization resistances might be lower than that of similar electrodes placed on the ScSZ electrolyte. The two systems experienced an increase value of R during the 100 h stability experiment at

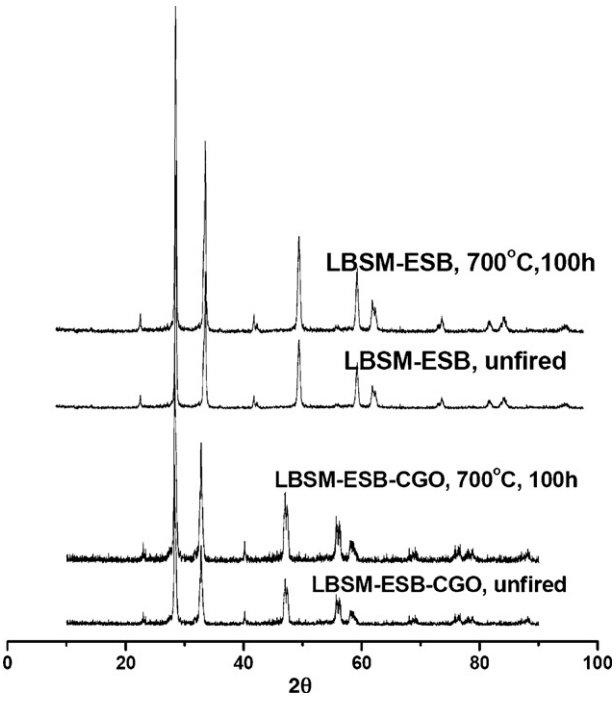

Fig. 9. The XRD spectra of LBSM–ESB powder mixtures and LBSM–ESB–CGO powder mixtures before and after co-firing at 700 °C for 100 h.

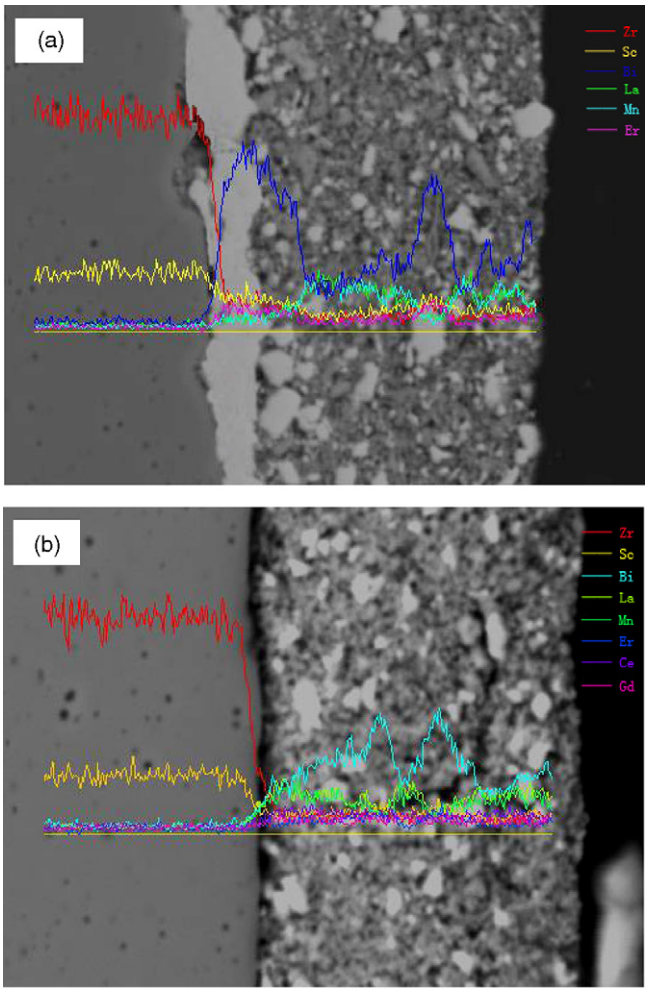

Fig. 10. EPMA cross-section images of the LBSM–ESB cathode on the ESB sintering function layer (a) and the LBSM–ESB–CGO10 cathode on the ScSZ electrolyte (b) after testing at 700 °C for 100 h.

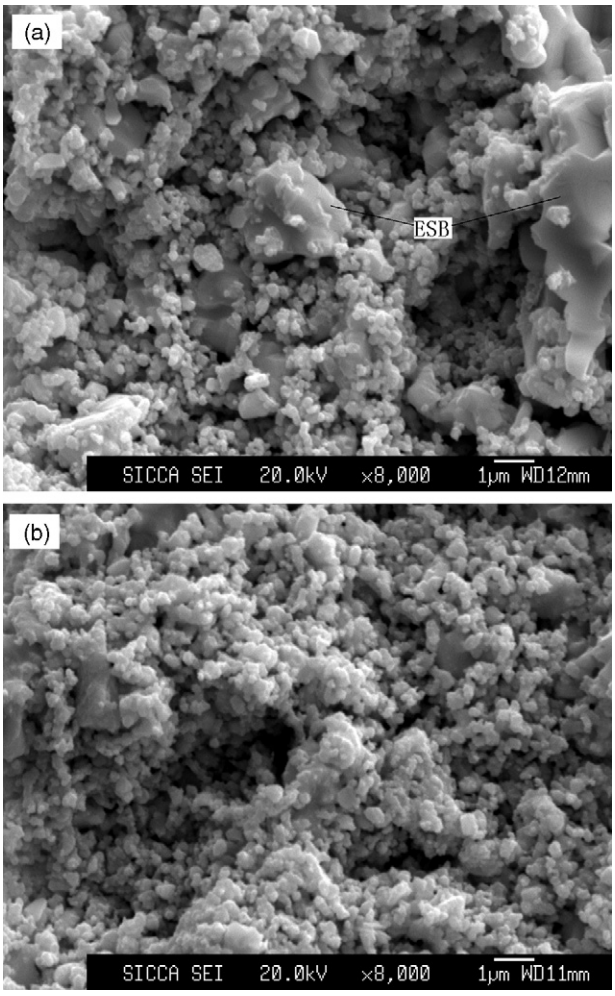

Fig. 11. Typical SEM fracture cross-section images of an LBSM–ESB cathode (a) and an LBSM–ESB–CGO10 cathode (b) after testing at 700 °C for 100 h.

open circuit, the polarization resistance (R) degraded at a rate of $2.15 \times 10^{-4}\ \Omega\,cm^2\,h^{-1}$ and $4.01 \times 10^{-5}\ \Omega\,cm^2\,h^{-1}$ for LBSM–ESB and LBSM–ESB–CGO10, respectively. The R values increased by 13% (from 0.165 $\Omega\,cm^2$ to 0.1865 $\Omega\,cm^2$) and 2.3% (from 0.177 $\Omega\,cm^2$ to 0.181 $\Omega\,cm^2$) for LBSM–ESB and LBSM–ESB–CGO10, respectively. The value of R for the LBSM–ESB electrode increased at a faster rate than that of the LBSM–ESB–CGO10 system. The X-ray diffraction patterns of the mixed LBSM and ESB powders (and mixed LBSM, ESB and CGO powders) before and after heat treatment at 700 °C for 100 h are shown in Fig. 9. The patterns reveal no evidence of inter-phase reactivity after heat treatment, so it can be inferred that each phase in the LBSM–ESB (or LBSM–ESB–CGO10) composite cathode is compatible and stable. Besides, Fig. 10 shows the results of EPMA testing on different samples, and it is concluded that no inter-diffusion has occurred between the different components. Thus, it is suspected that the growth and aggregation of the ESB phase is the major source of the observed increase in electrode polarization resistance, and the CGO particles can limit aggregation of the ESB phase.

The trends in electrode R shown in Fig. 8 can be rationalized in terms of the microstructure of the two different electrode systems after testing at 700 °C for 100 h (shown in Fig. 11). The LBSM–ESB system exhibits a relatively obvious growth and coalescence of the ESB phase after testing at 700 °C for 100 h, as seen by comparing Fig. 11a with Fig. 3d, which will further reduce the porosity and TPB length, and hence a smaller reaction zone for oxygen reduction. Further, increased density can lead to concentration polarization effects, where the reactive species (oxygen admolecules) are supplied to the reaction sites more slowly than they are consumed. However, as shown in Fig. 11b, there are few coalescent particles. It can be observed that there is hardly any change in the microstructure of LBSM–ESB–CGO10 after testing at 700 °C for 100 h by comparing Fig. 5b with Fig. 11b. So, it can be deduced that there is less growth and coalescence of the ESB phase in the LBSM–ESB–CGO10 electrode compared with the LBSM–ESB system, as the CGO phase helps to restrict the migration and ultimate aggregation of the ESB phase, and provides an electrode with a greater surface area. This is reflected in the one order slower rate of R increase for this composite system.

It may be possible to improve the performance of the cathode systems. For example, performance could be improved by optimizing the grain size in the composite cathodes. We could change the method of introducing ESB or CGO, such as by an ion-impregnating process instead of direct mixing. Xu et al. reported the ion-impregnating process to be very beneficial for cathode performance [25]. Besides, the operating temperature of the composite cathodes can be lowered, in which case the growth and aggregation of the ESB phase would be reduced and the stability of the composite cathodes further improved.

4. Conclusion

Reducing the cathode sintering temperature or the addition of 10 vol% nano-size CGO powders can lower the initial polarization resistance of the composite cathodes. We first attempted to introduce an ESB sintering function layer to reduce the sintering temperature of the LBSM–ESB cathode. However, this cathode has inadequate microstructure stability for long-term application at 700 °C, and the polarization resistance (R) degraded at a rate of $2.15 \times 10^{-4}\,\Omega\,cm^2\,h^{-1}$. The CGO powder in the LBSM–ESB–CGO10 cathode effectively improved the stability of the microstructure, and its R value was reduced at a rate of $4.01 \times 10^{-5}\,\Omega\,cm^2\,h^{-1}$. However, the stability of this cathode still needs improvement. It is likely that the growth and aggregation of the ESB phase will be suppressed further by reducing the ESB particle size and the operating temperature.

Acknowledgement

This work is supported financially by the Chinese High Technology Development Project (2007AA05Z151).

References

[1] N.Q. Minh, J. Am. Ceram. Soc. 76 (1993) 563–588.
[2] H.C. Yu, F. Zhao, A.V. Virkar, K.Z. Fung, J. Power Sources 152 (2005) 22–26.
[3] B.C.H. Steele, K.M. Hori, S. Uchino, Solid State Ionics 135 (2000) 445–450.
[4] B.C.H. Steele, Solid State Ionics 129 (2000) 95–110.
[5] N.P. Brandon, S. Skinner, B.C.H. Steel, Annu. Rev. Mater. Res. 33 (2003) 183–213.
[6] C. Xia, W. Rauch, F. Chen, M. Liu, Solid State Ionics 149 (1–2) (2002) 11–19.
[7] T. Horita, K. Yamaji, N. Sakai, Y. Xiong, T. Kato, H. Yokokawa, T. Kawada, J. Power Sources 106 (2002) 224–230.
[8] K. Sasaki, J. Tamura, H. Hosoda, T.N. Lan, K. Yasumoto, M. Dokiya, Solid State Ionics 148 (3–4) (2002) 551–555.
[9] S.H. Chan, C.F. Low, O.L. Ding, J. Power Sources 103 (2) (2002) 188–200.
[10] T. Horita, K. Yamaji, N. Sakai, H. Yokokawa, A. Weber, E. Ivers-Tiffée, Electrochim. Acta 46 (12) (2001) 1837–1845.
[11] T. Ishihara, T. Kudo, H. Matsuda, Y. Takita, J. Electrochem. Soc. 142 (5) (1995) 1519–1524.
[12] M. Mogensen, S. Skaarup, Solid State Ionics 86–88 (2) (1996) 1151–1160.
[13] M. Gödickemeier, K. Sasaki, L.J. Gauckler, I. Riess, Solid State Ionics 86–88 (2) (1996) 691–701.
[14] A. Jaiswal, E. Wachsman, Solid State Ionics 177 (2006) 677–685.
[15] M. Camaratta, E. Wachsman, Solid State Ionics 178 (2007) 1242–1247.
[16] C.R. Xia, Y.L. Zhang, M.L. Liu, Appl. Phys. Lett. 82 (2003) 901–903.
[17] H.X. Hu, M.L. Liu, J. Electrochem. Soc. 143 (1996) 859–862.
[18] A. Jaiswal, E. Wachsman, J. Electrochem. Soc. 152 (2005) A787–790.
[19] V. Esposito, B.H. Luong, E.D. Bartolomeo, E. Wachsman, E. Traversa, J. Electrochem. Soc. 153 (2006) A2232–2238.
[20] J.L. Li, S.R. Wang, Z.R. Wang, R.Z. Liu, T.L. Wen, Z.Y. Wen, J. Power Sources 179 (2008) 474–480.
[21] M.J. Jørgensen, S. Primdahl, C. Bagger, M. Mogensen, Solid State Ionics 139 (2001) 1–11.
[22] F.H. Heuveln, H.J.M. Bouwmeester, J. Electrochem. Soc. 144 (1997) 134–137.
[23] Y.J. Leng, S.H. Chan, K.A. Khor, S.P. Jiang, Int. J. Hydrogen Energy 29 (2004) 1025–1033.
[24] S.Y. Li, Z. Lü, N. Ai, K.F. Chen, W.H. Su, J. Power Sources 165 (2007) 97–101.
[25] X.Y. Xu, Z.Y. Jiang, X. Fan, C.R. Xia, Solid State Ionics 177 (2006) 2113–2117.